



**HAL**  
open science

## Mass measurement and isoscaling in $^{124}\text{Sn}+\text{Sn}$ and $^{107}\text{Sn}+\text{Sn}$ reactions at 600 AMeV

S. Bianchin, C. Sfienti, J. Lukasik, A. Le Fevre, W. Trautmann, P. Adrich, T. Aumann, C.O. Bacri, T. Barczyk, R. Bassini, et al.

### ► To cite this version:

S. Bianchin, C. Sfienti, J. Lukasik, A. Le Fevre, W. Trautmann, et al.. Mass measurement and isoscaling in  $^{124}\text{Sn}+\text{Sn}$  and  $^{107}\text{Sn}+\text{Sn}$  reactions at 600 AMeV. XLV International Winter meeting on Nuclear Physics, Jan 2007, Bormio, Italy. pp.233-242. in2p3-00165267

**HAL Id: in2p3-00165267**

**<https://in2p3.hal.science/in2p3-00165267v1>**

Submitted on 25 Jul 2007

**HAL** is a multi-disciplinary open access archive for the deposit and dissemination of scientific research documents, whether they are published or not. The documents may come from teaching and research institutions in France or abroad, or from public or private research centers.

L'archive ouverte pluridisciplinaire **HAL**, est destinée au dépôt et à la diffusion de documents scientifiques de niveau recherche, publiés ou non, émanant des établissements d'enseignement et de recherche français ou étrangers, des laboratoires publics ou privés.

# Mass measurement and isoscaling in $^{124}\text{Sn}+\text{Sn}$ and $^{107}\text{Sn}+\text{Sn}$ reactions at 600 AMeV

S. Bianchin<sup>1</sup>, C. Sfienti<sup>1</sup>, J. Lukasik<sup>1,7</sup>, A. Le Fèvre<sup>1</sup>, W. Trautmann<sup>1</sup>, P. Adrich<sup>1</sup>,  
T. Aumann<sup>1</sup>, C.O. Bacri<sup>2</sup>, T. Barczyk<sup>8</sup>, R. Bassini<sup>9</sup>, C. Boiano<sup>9</sup>, A.S. Botvina<sup>1,10</sup>,  
A. Boudard<sup>3</sup>, J. Brzychczyk<sup>8</sup>, A. Chbihi<sup>4</sup>, J. Cibor<sup>7</sup>, B. Czech<sup>7</sup>, M. De Napoli<sup>5</sup>, J. -E. Ducret<sup>3</sup>,  
H. Emling<sup>1</sup>, J. Frankland<sup>4</sup>, M. Hellström<sup>1</sup>, D. Henzlova<sup>1</sup>, K. Kezzar<sup>1</sup>, G. Immè<sup>5</sup>, I. Iori<sup>9</sup>,  
H. Johansson<sup>1</sup>, A. Lafriakh<sup>2</sup>, E. Le Gentil<sup>3</sup>, Y. Leifels<sup>1</sup>, W. G. Lynch<sup>1,11</sup>, J. Lühning<sup>1</sup>,  
U. Lynen<sup>1</sup>, Z. Majka<sup>8</sup>, M. Mocko<sup>11</sup>, W. F. J. Müller<sup>1</sup>, A. Mykulyak<sup>6</sup>, H. Orth<sup>1</sup>, A. N. Otte<sup>1</sup>,  
R. Palit<sup>1</sup>, P. Pawłowski<sup>8</sup>, A. Pullia<sup>9</sup>, G. Raciti<sup>5</sup>, E. Rapisarda<sup>5</sup>, H. Sann<sup>1</sup>, C. Schwarz<sup>1</sup>,  
H. Simon<sup>1</sup>, K. Sümmerer<sup>1</sup>, M. B. Tsang<sup>11</sup>, G. Verde<sup>11</sup>, C. Volant<sup>3</sup>, M. Wallace<sup>11</sup>, H. Weick<sup>1</sup>,  
J. Wiechula<sup>1</sup>, A. Wieloch<sup>8</sup> and B. Zwieglinski<sup>6</sup>,

## The ALADiN2000 Collaboration

- <sup>1</sup> Gesellschaft für Schwerionenforschung mbH (GSI), D-64291 Darmstadt, Germany  
<sup>2</sup> Institut de Physique Nucléaire, IN2P3-CNRS et Université, F-91406 Orsay, France  
<sup>3</sup> DAPNIA/SPhN, CEA/Saclay, F-91191 Gif-sur-Yvette, France  
<sup>4</sup> GANIL, CEA et IN2P3-CNRS, B.P. 55027, F-14076 Caen, France  
<sup>5</sup> Dipartimento di Fisica dell'Università and LNS-INFN, I-95126 Catania, Italy  
<sup>6</sup> A. Soltan Institute for Nuclear Studies, PL-00681 Warsaw, Poland  
<sup>7</sup> H. Niewodniczański Institute of Nuclear Physics, PL-31342 Kraków, Poland  
<sup>8</sup> M. Smoluchowski Institute of Physics, Jagiellonian Univ., PL-30059 Kraków, Poland  
<sup>9</sup> Istituto di Scienze Fisiche, Università degli Studi and INFN, I-20133 Milano, Italy  
<sup>10</sup> Inst. Nucl. Res., Russian Academy of Science, Ru-117312 Moscow, Russia  
<sup>11</sup> Department of Physics and Astronomy and NSCL, MSU, East Lansing, MI 48824 USA

## Abstract

Isotopic effects in projectile spectator fragmentation at 600 AMeV have been investigated using data collected in recent experiments with SIS beams at the GSI laboratory and with the ALADiN forward-spectrometer. For this purpose, primary beams of  $^{124}\text{Sn}$ , as well as secondary beams of  $^{124}\text{La}$  and  $^{107}\text{Sn}$  produced at the FRS fragment separator have been used. Isoscaling in  $^{124,107}\text{Sn}+\text{Sn}$  reactions is investigated and results are compared with data taken with the INDRA multidetector for  $^{12}\text{C}+^{112,124}\text{Sn}$  reactions.

## 1 Introduction

The growing interest in isospin effects in nuclear reactions is motivated by an increasing awareness of the importance of the symmetry term in the nuclear equation of state, in particular for astrophysical applications. Supernovæ simulations or neutron star models require inputs for the nuclear equation of state at extreme values of density and asymmetry for which the predictions differ widely [1, 2]. Fragmentation reactions are, therefore, a very interesting tool because they permit the production of nuclear systems with subnuclear densities and temperatures which,

*e.g.*, largely overlap with those expected for the explosion stages of core-collapse supernovæ [3]. Laboratory studies of the properties of nuclear matter in the hot environment, similar to the astrophysical situation, are thus becoming feasible, and an active search for suitable observables is presently underway. Of particular interest is the density-dependent strength of the symmetry term which is essential for the description of neutron-rich objects up to the extremes encountered in neutron stars. In a very recent experiment with the ALADiN spectrometer, the possibility of using secondary beams for reaction studies at relativistic energies has been explored. Beams of  $^{107}\text{Sn}$ ,  $^{124}\text{Sn}$ ,  $^{124}\text{La}$ , and  $^{197}\text{Au}$  as well as Sn and Au targets were used to investigate the mass and isospin dependence of projectile fragmentation at 600 MeV per nucleon. The neutron-poor radioactive projectiles  $^{107}\text{Sn}$  and  $^{124}\text{La}$  were produced at the Fragment Separator FRS.

The present contribution will show results obtained from an isoscaling analysis with the collected data. A comparison will be made with data obtained with the  $4\pi$  multidetector INDRA and the relation between isoscaling and the coefficient  $\gamma$  of the symmetry-energy term  $E_{\text{sym}} = \gamma(A - 2Z)^2/A$  will be discussed.

## 2 The S254 experiment

The S254 experiment has been devoted to the investigation of isotopic effects in the decay of projectile spectators at relativistic energies. For this purpose, fragment decays of  $^{197}\text{Au}$ ,  $^{124}\text{Sn}$ ,  $^{107}\text{Sn}$  and  $^{124}\text{La}$  projectiles in collisions with  $^{\text{nat}}\text{Sn}$  and Au targets at an incident energy  $E=600$  AMeV have been studied with the ALADiN (A large Acceptance Dipole magNet) forward-spectrometer at SIS.

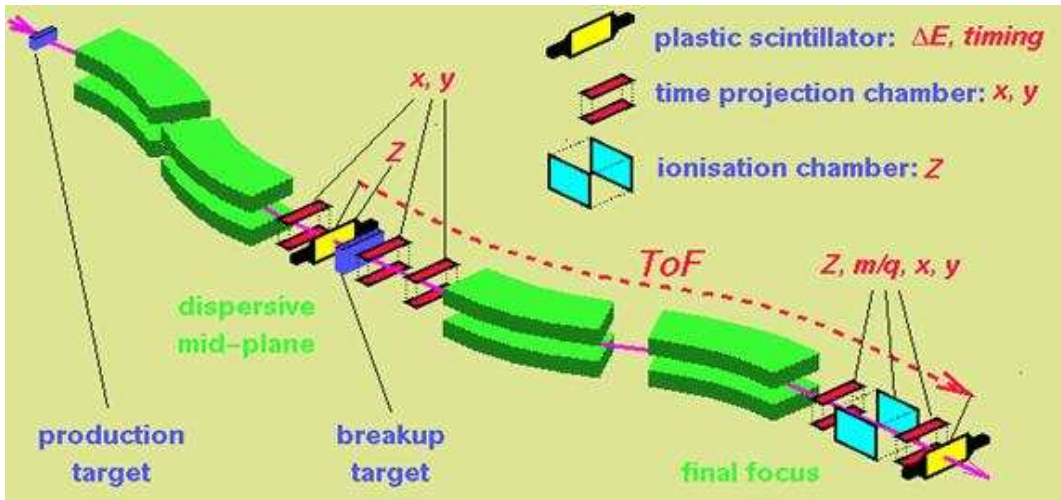


Figure 1: Schematic view of the fragment separator FRS.

### 2.1 Production of secondary beams

In order to extend the range of isotopic compositions of the excited spectator systems, four different projectiles, all with incident energy of 600 MeV per nucleon, have been investigated allowing a study of various combinations of masses and  $N/Z$  ratios in the entrance channel:

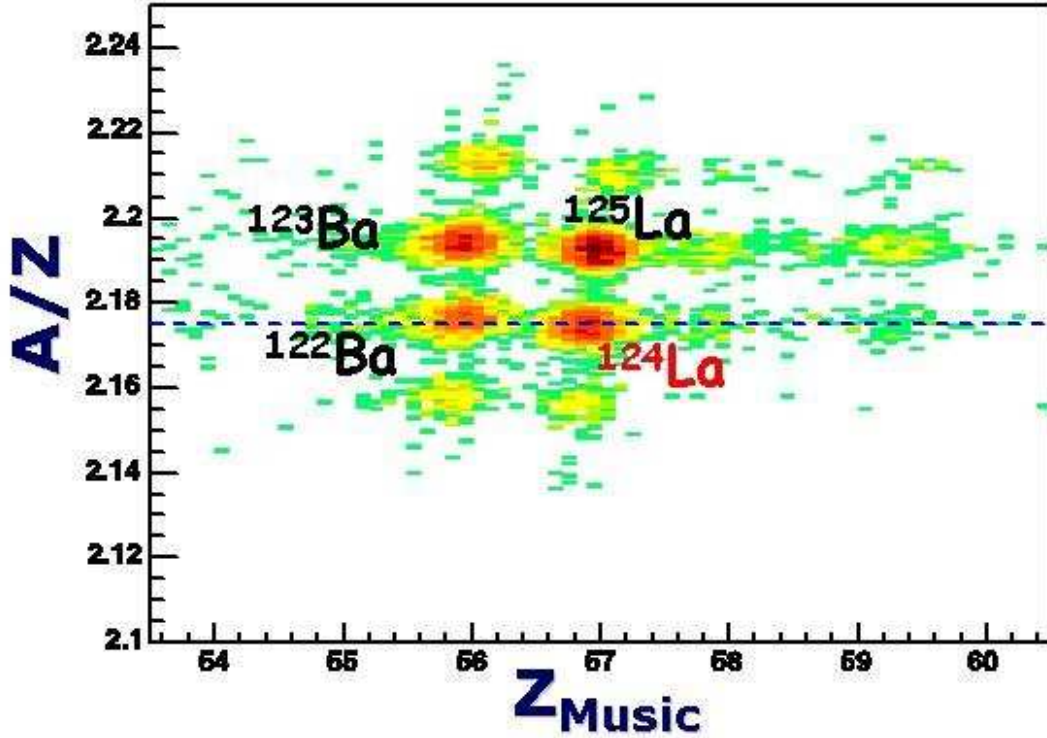


Figure 2: Event distribution in the plane  $A/Z$  vs  $Z_{\text{MUSIC}}$  for a nominal beam of  $^{124}\text{La}$ .

$^{124}\text{Sn}$ ,  $^{197}\text{Au}$ ,  $^{124}\text{La}$  and  $^{107}\text{Sn}$ . The two latter beams have been delivered by the FRagment Separator (FRS) of the GSI laboratory as products of the fragmentation of primary  $^{142}\text{Nd}$  beams at 895 and 875 AMeV on a  $^9\text{Be}$  production target with a density of  $4009 \text{ mg/cm}^2$ . The separation and the focusing of the fragments produced by the reaction take place in the four different parts of the fragment separator. Each of these parts is composed of a dipole magnet used to separate the different ion species as a function of their  $A/Z$  ratio and two quadrupole magnets used for focusing (Fig. 1). Although the fragment separator is able to provide an isotopically pure secondary beam using a wedge-shaped degrader to select the charge of the desired beam, we have chosen not to use it, in order to maintain a beam intensity of approximately 2000 particles/sec. The position measurement at the dispersive mid-plane and the measurement of the flight time during the 80 m passage from the FRS to the ALADiN spectrometer permit the reconstruction of the  $A/Z$  ratio of the selected projectiles with high precision. A discriminant analysis using information from all upstream detectors permits a selection of  $Z_{\text{proj}}$  with good resolution, if necessary. As an illustration, the composition of the beam delivered by the fragment separator is shown in Fig. 2. In the present analysis, the secondary beam delivered by the fragment separator is used without any further selection.

## 2.2 The ALADiN spectrometer

A schematic layout of the experimental setup is shown in Fig. 3. For each beam particle, its arrival time and its position in a plane perpendicular to the beam direction are measured upstream of the target with two thin plastic scintillators. The geometric acceptance of the spectrometer is  $\theta_{lab} \approx \pm 9.2^\circ$  horizontally and  $\pm 4.3^\circ$  vertically. It is matched by the dimensions of the Time Projection-MULTiple Sampling Ionization Chamber TP-MUSIC IV and by the time-of-flight (TOF) wall. At  $E=600$  AMeV, the angular distributions of some lighter fragments extend beyond the acceptance of the spectrometer and are detected in the CsI(Tl) hodoscope array that surrounds the entrance of the magnet. The Large Area Neutron Detector LAND [4], used to determine the neutron multiplicity, is positioned close to zero degrees with respect to the incident beam direction.

The atomic numbers  $Z$  and the velocities of nuclear fragments are determined with the TOF wall, located at the end of the ALADiN spectrometer and extending over 2.4 m in horizontal and 1.0 m in vertical directions. It consists of two layers of vertically mounted scintillator strips of 2.5 cm width and 1.0 cm thickness, viewed by photomultiplier tubes at both ends [5]. The two layers are offset by half a width with respect to each other. The primary beam is directed through a hole of  $4.8 \times 6.0$  cm<sup>2</sup> cut into the middle sections of the central scintillator modules. An overall time resolution of about 400 ps and 120 ps (FWHM) for fragments with  $Z=2$  and  $Z \approx Z_{proj}$ , respectively, is achieved. The TP-MUSIC IV detector used to measure the charge

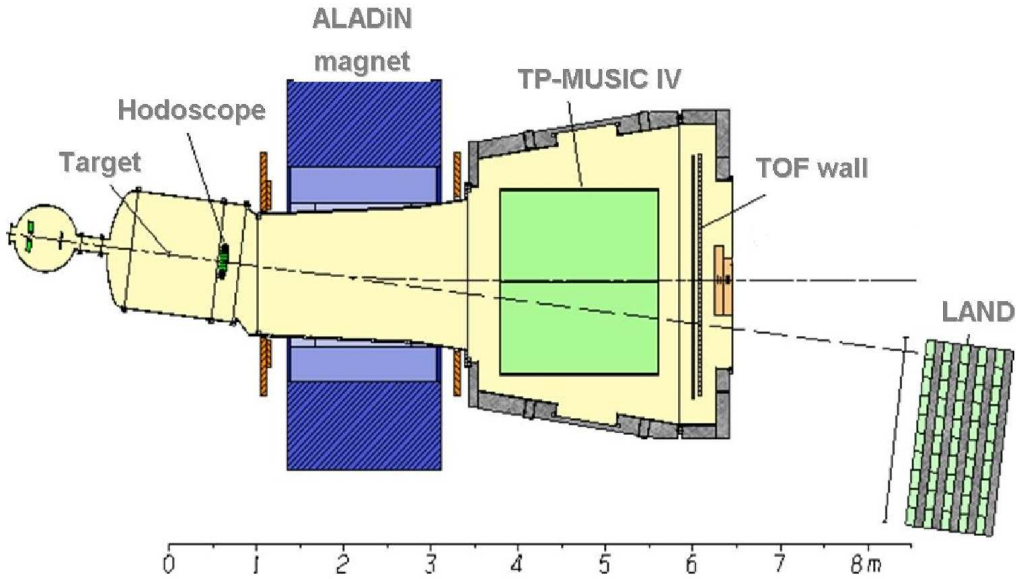


Figure 3: Cross sectional view of the ALADiN spectrometer. The beam enters from the left and is monitored by two beam detectors before reaching the target. Projectile fragments entering into the acceptance of the magnet are tracked and identified in the TP-MUSIC IV detector and in the time of flight (TOF) wall. Fragments and particles emitted in forward directions outside the magnet acceptance and up to  $\theta_{lab} = 16^\circ$  are detected in the CsI(Tl) array. Neutrons emitted in directions close to  $\theta_{lab} = 0^\circ$  are detected with the Large Area Neutron Detector (LAND). The dashed line indicates the direction of the incident beam. The dash-dotted line represents the trajectory of beam particles after they were deflected by an angle of  $7.3^\circ$ .

and to reconstruct the trajectory of the projectile fragments, is divided into two parts separated by a cathode plane. On each side of the detector, three ionisation chamber sections (each with 8 anodes) and four proportional counters are used. Using charge-division and pads techniques, the TP-MUSIC IV allows the reconstruction of the trajectories of the fragments.

### 3 Trajectory reconstruction

Isoscaling requires the knowledge of the isotopic composition of the fragments produced in the collisions. It is, therefore, necessary to determine precisely the mass of each of these fragments, which is achieved by reconstructing their trajectory through the known field of the ALADiN magnet. This procedure allows us to determine the magnetic rigidity of the reaction products and, with the measured charge and velocity, their mass.

The reconstruction is based on the so-called *backtracking method*. The trajectories of the fragments inside the TP-MUSIC IV are deduced from their positions measured with the proportional counters. With an assumed starting value for the rigidity, this trajectory is followed back through the magnet. In an iterative procedure, the fragment rigidity is varied until the reconstructed intersection with the target plane coincides with the intersection of the projectile, measured with an accuracy of about 1 mm. A fragment entering in the acceptance of a magnet is deflected along a trajectory of radius  $\rho$  (in unit of meter) given by:

$$|\vec{R}| = B\rho = \frac{p}{0.3q} \quad (1)$$

where the magnetic field  $B$ , the charge of the fragment  $q$  and its momentum  $p$  are given in units of Tesla, electron charge and  $GeV/c$ , respectively. Since the momentum of the fragment is given by:

$$p = m_0\beta\gamma A = \frac{m_0\beta A}{\sqrt{1-\beta^2}} \quad (2)$$

with  $m_0=0.935$  GeV/ $c^2$ , the mass number  $A$  and  $\beta = v/c$ , it follows that:

$$A = \frac{0.3Z|\vec{R}|\sqrt{1-\beta^2}}{m_0\beta} \quad (3)$$

The rigidity  $|\vec{R}|$  is measured with a resolution of  $\sim 1$  % for  $Z = Z_{\text{proj}}$  through the trajectory reconstruction procedure, the charge  $Z$  is measured by both the TP-MUSIC IV detector and the TOF-wall and the velocity  $\beta$  is obtained measuring the time-of-flight with the TOF-wall knowing the path length from the reconstruction of the trajectory. Fig. 4 shows mass spectra obtained for light fragments ( $2 \leq Z \leq 10$ ) produced by the fragmentation of  $^{124}\text{Sn}$  (upper panels) and  $^{107}\text{Sn}$  (lower panels) projectiles on a  $^{\text{nat}}\text{Sn}$  target. The mass resolution obtained for fragments entering into the acceptance of the ALADiN spectrometer is about  $\Delta A/A = 3$  % (FWHM) for fragments with  $Z=2$  and decreases to 1.5 % for  $Z \geq 8$ . Masses are thus individually resolved for fragments with atomic number  $Z \leq 10$ . The dominant contribution to the uncertainty of the mass measurement:

$$\frac{\Delta A}{A} = \sqrt{\left(\frac{\Delta R}{R}\right)^2 + \left(\gamma^2 \frac{\Delta t}{t}\right)^2} \quad (4)$$

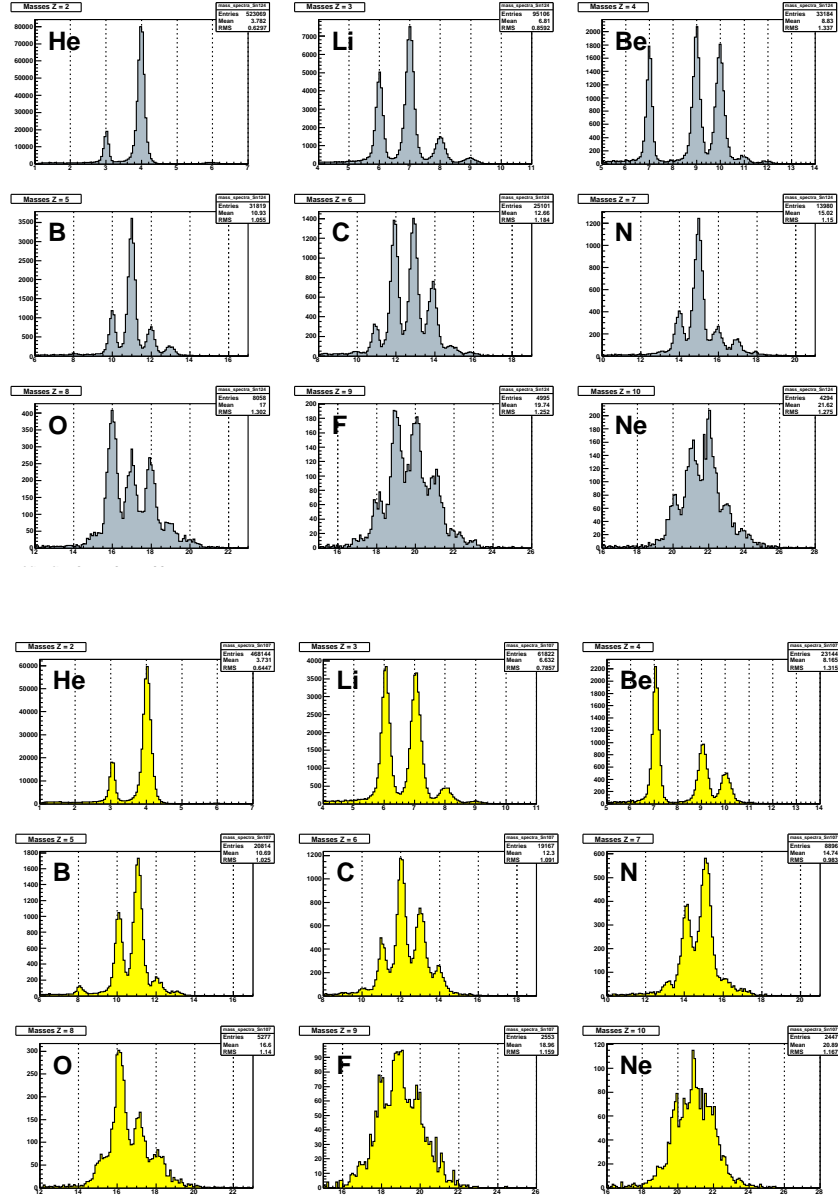


Figure 4: Mass spectra obtained by reconstructing fragment trajectories and time-of-flights for  $^{124}\text{Sn}+\text{Sn}$  (upper panels) and  $^{107}\text{Sn}+\text{Sn}$  (lower panels) at 600 MeV per nucleon for fragments with charge  $2 \leq Z \leq 10$ .

is caused by the mass-dependent error for the time measurement which is amplified by the factor  $\gamma^2$  (for 600 MeV/nucleon,  $\gamma^2=2.6$ ). Assuming that the rigidity resolution is about 1 % for  $Z_{\text{proj}}$ , a time resolution of  $\Delta t \approx 280$  ps (FWHM) can be deduced for the light fragments and  $\Delta t \approx 120$  ps (FWHM) for the projectile. By inspection of the mass spectra, first-order isotopic effects can be observed: higher yields are obtained for neutron-rich isotopes in the case of the neutron-rich system.

## 4 Isoscaling and symmetry energy

Isotopic scaling, also called *isoscaling*, has been shown to be a phenomenon common to many different types of heavy-ion reactions [6-9]. It is observed by comparing products yields  $Y_i$  from reactions which differ only in the isotopic composition of the projectiles or targets or both but are otherwise identical. Isoscaling refers to an exponential dependence of the measured yield ratios  $R_{21}(N, Z)$  on the neutron number  $N$  and the proton number  $Z$  of the detected products. The scaling expression

$$R_{21}(N, Z) = Y_2(N, Z)/Y_1(N, Z) = C \exp(\alpha N + \beta Z) \quad (5)$$

describes rather well the measured ratios over a wide range of complex particles and light fragments [10]. For illustration, the yield ratios  $R(\text{Sn124}/\text{Sn107})$  obtained for the fragmentation

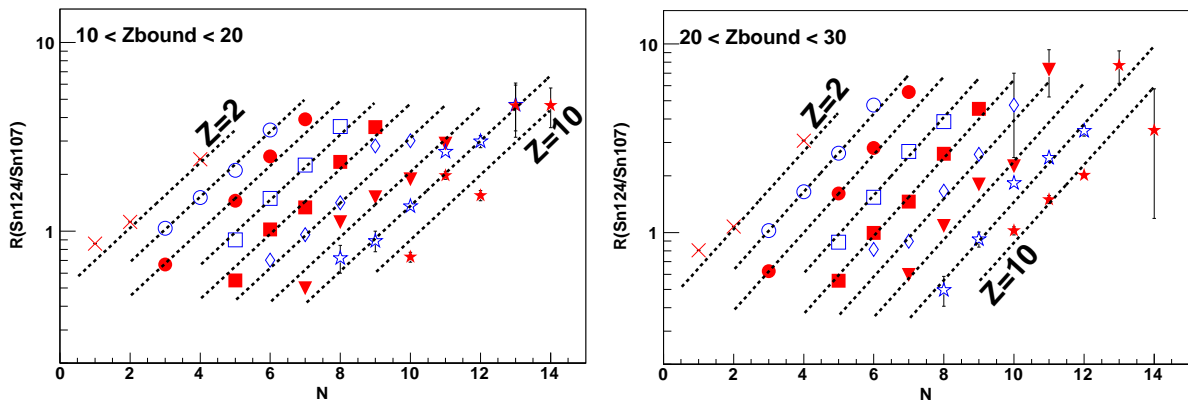


Figure 5: Yield ratios for He to Ne isotopes from the fragmentation of  $^{124}\text{Sn}$  and  $^{107}\text{Sn}$  projectiles at 600 AMeV as a function of the neutron number  $N$  for two different centrality selections. The dashed lines are the results of exponential fits (for elements with  $3 \leq Z \leq 10$ ) according to Eq. (5).

of the  $^{124}\text{Sn}$  and  $^{107}\text{Sn}$  projectiles in the  $Z_{\text{bound}} = 10 - 20$  and  $Z_{\text{bound}} = 20 - 30$  intervals, covering the region of maximum fragment production, are plotted in Fig. 5 as a function of the neutron number. Isotopes of the same elements are plotted with the same symbols. Odd- $Z$  nuclei are represented by open symbols while even- $Z$  nuclei are represented by closed symbols (helium isotopes are represented by a cross). The dashed lines are best fits to the data points with one common pair of values  $\alpha$  and  $\beta$  for elements with  $3 \leq Z \leq 10$ . In the case of Fig. 5,  $\alpha=0.397$  and  $\alpha=0.476$  for  $Z_{\text{bound}} = 10 - 20$  and  $Z_{\text{bound}} = 20 - 30$ , respectively. The fit values for other centrality selections are reported in Table 1. The observable  $Z_{\text{bound}}$ , defined as the sum of the charges of the projectile fragments ( $Z \geq 2$ ) and used to sort the collisions according to their centrality, is related to the impact parameter and, thus, to the excitation energy. The accuracy of the isoscaling described by Eq. (5) can be compactly displayed, and then more easily judged, by plotting the scaled isotopic ratio, as a function of the neutron number  $N$ ,

$$S(N) = R_{12}(N, Z) \exp(-\beta Z) \quad (6)$$



$Z_{\text{bound}}$	$\alpha$	$\beta$
0-10	$0.320 \pm 0.005$	$-0.343 \pm 0.001$
10-20	$0.397 \pm 0.001$	$-0.416 \pm 0.001$
20-30	$0.476 \pm 0.001$	$-0.497 \pm 0.001$
30-40	$0.633 \pm 0.002$	$-0.648 \pm 0.002$
40-50	$0.826 \pm 0.082$	$-0.888 \pm 0.039$

Table 1: Parameters obtained from fitting the measured isotopic yield ratios with the scaling function given by Eq. (5) as a function of the  $Z_{\text{bound}}$  selection (i.e. of the excitation energy). The first and last intervals are fitted for  $3 \leq Z \leq 8$ , whereas the other ones are fitted for  $3 \leq Z \leq 10$ .

For all elements,  $S(N)$  should lie along a straight line on a semilog plot when Eq. (5) accurately describes the experimental data.

The scaled isotopic ratio  $S(N)$  for different centrality selections obtained for the S254 experiment is shown in Fig. 6 (left panel). For a comparison, data obtained with the INDRA  $4\pi$  detector for  $^{12}\text{C}$  on  $^{112,124}\text{Sn}$  reactions at incident energies of 300 and 600 MeV per nucleon are also plotted [11]. The difference between the isotopic compositions of the two systems being smaller in the case of the INDRA experiment, the value of the scaling parameter  $\alpha$ , for a given centrality, is, as expected, smaller than in the present experiment. However, normalized by the difference of the squared  $Z/A$  values (see below), we obtain for the most peripheral bins  $\alpha/\Delta(Z^2/A^2)=14.1$  and  $\alpha/\Delta(Z^2/A^2)=15.8$  for the INDRA and the present experiments, respectively. This represents an agreement within  $\sim 10\%$ .

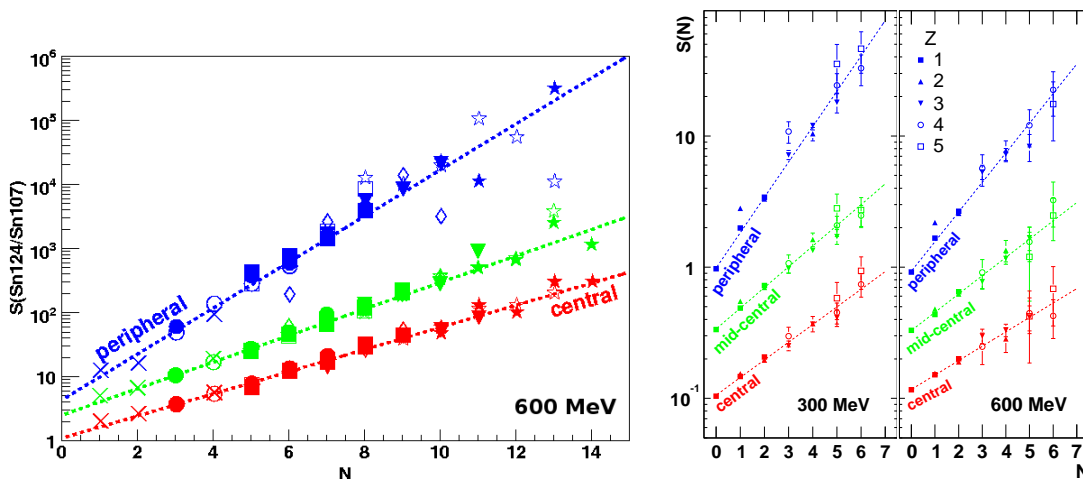


Figure 6: Scaled isotopic ratios  $S(N)$  for  $^{107,124}\text{Sn}+\text{Sn}$  at  $E=600$  AMeV (left panel) and for  $^{12}\text{C}+^{112,124}\text{Sn}$  at  $E=300$  AMeV and  $600$  AMeV obtained with the INDRA multidetector (right panel) [11] for three different centralities. In both cases, the dashed lines are the results of exponential fits according to Eq. (5).

The slope parameter  $\alpha$  decreases strongly with the centrality of the collision, extending from  $\alpha=0.826$  to  $\alpha=0.320$  for the most central event group (Table 1). The  $^{12}\text{C}$  induced reactions cover the rise of fragment production over the range up to  $Z_{\text{bound}} \approx Z_{\text{proj}}/2$ , whereas for collisions with the Sn target (in inverse kinematics) this range extends to very small  $Z_{\text{bound}}$ . Moreover, in the INDRA case, the centrality selection was based on charged-particle multiplicity and not on  $Z_{\text{bound}}$ , which makes the comparison between the two experiments not straightforward. Central collisions in  $^{12}\text{C}$  induced reactions correspond, approximately, to the bin 20-30 in the present experiment. In both cases,  $\alpha$  has about half the value observed for peripheral collisions. The present data show that  $\alpha$  decreases even further for the more violent collisions initiated with the Sn target.

In the grand-canonical approximation, assuming that the temperature  $T$  is about the same, the scaling parameters  $\alpha$  and  $\beta$  are proportional to the difference of the neutron and proton chemical potentials for the two systems divided by the temperature,  $\alpha = \Delta\mu_n/T$  and  $\beta = \Delta\mu_p/T$ . Of particular interest is their connection with the coefficient  $\gamma$  of the symmetry-energy term  $E_{\text{sym}} = \gamma(A - 2Z)^2/A$ , which has been obtained from the statistical interpretation of isoscaling within the SMM [7] and expanding-emitting-source model [10] and confirmed by an analysis of reaction dynamics [12]. The relation is

$$\alpha T = \Delta\mu_n = \mu_{n,2} - \mu_{n,1} \approx 4\gamma \left( \frac{Z_1^2}{A_1^2} - \frac{Z_2^2}{A_2^2} \right) = 4\gamma\Delta(Z^2/A^2) \quad (7)$$

where  $Z_1$ ,  $A_1$  and  $Z_2$ ,  $A_2$  are the charges and mass numbers of the neutron-poor and neutron-rich systems at breakup, respectively. The coefficient  $\gamma$  of the symmetry term can then be obtained from isoscaling knowing the temperature and the isotopic compositions [11]. For this purpose, temperature measurements using isotopic thermometers are currently being investigated with data collected during the S254 experiment [13]. The difference of the chemical potentials also depends on the isotopic composition at breakup. Although transport models predict that the difference between isotopic compositions for the two systems should not deviate by more than a few percent from the original value [14], larger deviations would have a significant effect on the deduced  $\gamma$ .

## 5 Summary and outlook

Isotopic effects in the projectile fragmentation have been studied with the ALADiN spectrometer at the GSI laboratory. Neutron-poor secondary beams produced at the fragment separator FRS have been used in addition to stable beams in order to cover a larger range of isotopic compositions. Resolved masses have been obtained for light fragments ( $2 \leq Z \leq 10$ ) by measuring their charge, their time-of-flight and by reconstructing their trajectory, allowing to distinguish unambiguously each isotope. Isoscaling has been observed for  $^{107,124}\text{Sn}+\text{Sn}$  reactions at 600 MeV per nucleon and the relation between the scaling parameter  $\alpha$  and the centrality of the collision has been shown. It confirms results obtained earlier with the INDRA multidetector for  $^{12}\text{C}+^{112,124}\text{Sn}$  reactions at incident energies 300 and 600 AMeV and demonstrates that, as expected, the value of the scaling parameter  $\alpha$  increases with the difference between the isotopic compositions of the two systems. The connection with the symmetry-energy term of the nuclear equation of state has

been discussed. The temperatures at breakup are currently being investigated using the double-isotope thermometer in order to quantitatively establish the evolution of the symmetry term [13].

*This work was supported by the European Community under contract No. HPRI-CT-1999-00001.*

## References

- [1] Bao-An Li, Phys. Rev. Lett. **88**, (2002) 192701.
- [2] A.S. Botvina and I.N. Mishustin, Phys. Lett. B **584**, (2004) 233.
- [3] A.S. Botvina and I.N. Mishustin, Phys. Rev. C **72**, (2005) 048801.
- [4] Th. Blaich *et al.*, Nucl. Instrum. Methods A **314**, (1992) 136.
- [5] J. Hubele *et al.*, Z. Phys. A **340**, (1991) 263.
- [6] M.B. Tsang *et al.*, Phys. Rev. Lett. **86**, (2001) 5023.
- [7] A.S. Botvina, O.V. Lozhkin and W. Trautmann, Phys. Rev. C **65**, (2002) 044610.
- [8] G.A. Souliotis *et al.*, Phys. Rev. C **68**, (2003) 024605.
- [9] W.A Friedman, Phys. Rev. C **69**, (2004) 031601(R).
- [10] M.B. Tsang *et al.*, Phys. Rev. C **64**, (2001) 054615.
- [11] A. Le Fèvre *et al.*, Phys. Rev. Lett. **94**, (2005) 162701.
- [12] A. Ono *et al.*, Phys. Rev. C **68**, (2003) 051601(R).
- [13] C. Sfienti *et al.*, Contribution to this proceeding.
- [14] T. Gaitanos *et al.*, Nucl. Phys. A **732**, (2004) 24.